ARTICLE   OPEN

Electronic localization in CaVO₃ films via bandwidth control

Daniel E. McNally[1], Xingye Lu [1], Jonathan Pelliciari[1,6], Sophie Beck[2], Marcus Dantz[1], Muntaser Naamneh[1], Tian Shang[1,3], Marisa Medarde[4], Christof W. Schneider[5], Vladimir N. Strocov[1], Ekaterina V. Pomjakushina[4], Claude Ederer[2], Milan Radovic[1] and Thorsten Schmitt[1]

Understanding and controlling the electronic structure of thin layers of quantum materials is a crucial first step towards designing heterostructures where new phases and phenomena, including the metal-insulator transition (MIT), emerge. Here, we demonstrate control of the MIT via tuning electronic bandwidth and local site environment through selection of the number of atomic layers deposited. We take $CaVO_3$, a correlated metal in its bulk form that has only a single electron in its V^{4+} 3d manifold, as a representative example. We find that thick films and ultrathin films (≤6 unit cells, u.c.) are metallic and insulating, respectively, while a 10 u.c. $CaVO_3$ film exhibits a clear thermal MIT. Our combined X-ray absorption spectroscopy and resonant inelastic X-ray scattering (RIXS) study reveals that the thickness-induced MIT is triggered by electronic bandwidth reduction and local moment formation from V^{3+} ions, that are both a consequence of the thickness confinement. The thermal MIT in our 10 u.c. $CaVO_3$ film exhibits similar changes in the RIXS response to that of the thickness-induced MIT in terms of reduction of bandwidth and V 3d–O 2p hybridization.

INTRODUCTION

Deposition methods with unit cell thickness precision enable new approaches to control the degree of electronic localization in quantum materials. For instance, epitaxial strain changes the lattice parameters altering the potential landscape of the electrons, dimensionality tunes the electronic bandwidth and interfacing provides a charge reservoir. Thickness-dependent metal-insulator transitions (MIT) in thin films have been widely reported in recent years in a broad swathe of correlated 3d and 5d transition metal oxides.[1–7] Understanding and controlling the electronic structure of these quantum materials is a critical first step toward designing heterostructures where new emergent phases and phenomena, including MIT, have been widely predicted.[8,9] The focus of our interest is to resolve the nature of the thickness-induced MIT, therefore, in this work we consider $CaVO_3$ as a model system.

Bulk $CaVO_3$ with a formal valence shell configuration of $V3d^1$ (V^{4+} oxidation state) is a paramagnetic metal with enhanced Sommerfeld-Wilson and Kadowaki-Woods ratios suggesting electronic correlations are important.[10] However, as is often the case for metals, neither moderate doping nor pressure induce insulating or magnetic ground states.[11,12] In contrast to the bulk, enhanced electron correlation strength and a MIT have recently been reported for $CaVO_3$ films of 20 unit cells (u.c.) or less.[6,13] While these discoveries are promising for technological applications such as transparent conductors[13] and MottFETs,[14,15] a complete understanding of the MIT in $CaVO_3$ has, until now, remained elusive.

Figure 1 illustrates that electronic bandwidth can control the degree of electron localization in $3d^1$ perovskites RXO_3. In the example presented in the top panels, applicable for bulk-like materials, when the orthorhombic distortion is increased the bandwidth decreases by up to 40% and a MIT occurs.[16] However, realising this MIT requires the substitution of both R and X ions making it very difficult to continuously control in practice. In our work presented here, we show that the bandwidth can be continuously controlled by up to 40% in $CaVO_3$ simply by choosing the number of atomic layers deposited on a $SrTiO_3$ substrate as summarized in the bottom panels of Fig. 1 and outlined in detail in the rest of this work.

RESULTS

MIT in thin film $CaVO_3$

Figure 2a presents electrical resistance as a function of temperature for our $CaVO_3$ and $SrVO_3$ thin films grown by pulsed laser deposition (PLD) on $SrTiO_3$ (100) substrates. The film thicknesses and surface ordering were routinely monitored with single-layer accuracy by reflection high-energy electron diffraction (RHEED), see Fig. 1 in S.I. For the thinner films (15 u.c., 10 u.c., 6 u.c., 4 u.c. $CaVO_3$) a thin 2 nm $SrTiO_3$ overlayer was deposited to protect against environmental (in air) degradation upon removal from PLD chamber. The thick 50 u.c. films are metallic at all temperatures, like bulk $CaVO_3$ and $SrVO_3$.[10,17] When the $CaVO_3$ (CVO) film thickness is reduced an MIT occurs. The 15 and 10 u.c. films undergo an MIT at 160 and 220 K, respectively, while the 6 and 4 u.c. films are insulating at all temperatures (the 4 u.c. film was too insulating to be measured using our setup). The overall behaviour is similar to that previously reported for $CaVO_3$ films.[6] Comparison of RHEED patterns recorded at room temperature
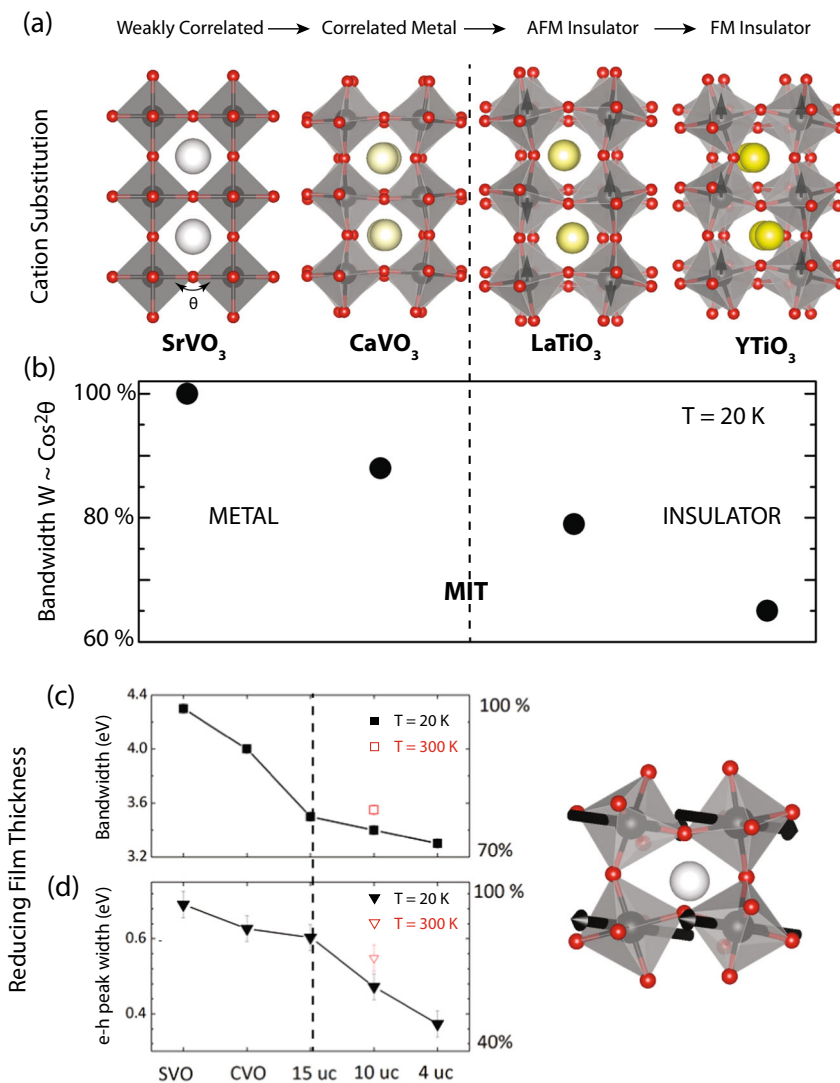
Fig. 1 Comparison of bandwidth change with cation substitution in bulk 3d^1 crystals with that realized in thin films of CaVO$_3$ by reducing film thickness. **a, b** The crystal structure and electronic bandwidth of different 3d^1 perovskites RXO$_3$ is presented. For R = Sr and X = V a cubic structure is reported. When R is substituted to R = Ca an orthorhombic distortion occurs changing the electronic bandwidth and local V site symmetry. This results in a more correlated metallic state. When R is substituted to R = La and X substituted to X = Ti (to maintain 3d^1 configuration), the distortion is further increased and a metal-insulator transition occurs (MIT). The MIT is accompanied by long range antiferromagnetic order that can be switched to ferromagnetic by substituting R to R = Y. **c, d** A comparable reduction in bandwidth is found when the MIT in CaVO$_3$ is controlled by film thickness as described in this manuscript

after deposition of 15 u.c. CVO (metallic at room temperature) and 6 u.c. CVO (insulating at room temperature) films suggests structural transitions (possibly octahedral rotation) to play a role in the thickness-induced MIT (see S.I. Figure 3). We emphasize that this structural reconstruction was only observed for the very thin CaVO$_3$ film of 6 u.c. thickness that was capped by a 2 nm (5. u.c.) SrTiO$_3$ over-layer (compare Figs 1 and 3 in S.I.). We ascribe an important role to the SrTiO$_3$ over-layer in inducing and/or stabilizing this structural reconstruction.

X-ray absorption (XAS) at the V L$_{2,3}$ edges, presented in Fig. 2b, reveals an evolution from broad d-bands and large valence fluctuations in metallic thick films of CaVO$_3$ to a more localized 3d character in the thinner insulating films. XAS of the thick metallic 50 u.c. film (red line) is similar to that of a CaVO$_3$ single crystal (brown), as well as a 50 u.c. SrVO$_3$ film (dashed black). These spectra are not well reproduced by multiplet calculations because of the itinerant character of the 3d electrons.[18] With reduced film thickness the XAS spectra become sharper, the L$_3$ peak energy is reduced by ~0.5 eV, a shoulder appears on the L$_3$ peak and a new

peak is found in the dip between L$_3$ and L$_2$ peaks. These new peaks are commonly observed in insulating VO$_2$ (V^{4+}, dashed grey) and V$_2$O$_3$ (V^{3+}) compounds (dashed magenta).[19] In particular, XAS of the thinner most insulating CaVO$_3$ films (6 and 4 u.c.) is similar to that reported for Y$_{1-x}$Ca$_x$VO$_3$ ($x \geq 0.6$) that contains a mixture of V^{4+} and V^{3+} character.[18] The increase in V^{3+} results from charge redistribution in the thinner films and is consistent with a reduced Madelung potential and hence reduced V–O covalency across the MIT. The sharpening of the L$_{2,3}$ peaks across the MIT reflects a reduction in the bandwidth of the upper Hubbard band. XAS of the 10 u.c. film in the high temperature metallic state is presented as a dashed blue curve in Fig. 2b. A broadening of the spectral features is observed with respect to the low temperature insulating state but the overall response is still different from that of the metallic thick 50 u.c. CaVO$_3$ film. We undertook a series of resonant inelastic X-ray scattering (RIXS) measurements to investigate further the change in the electronic excitations across the thickness-induced and thermal MIT.
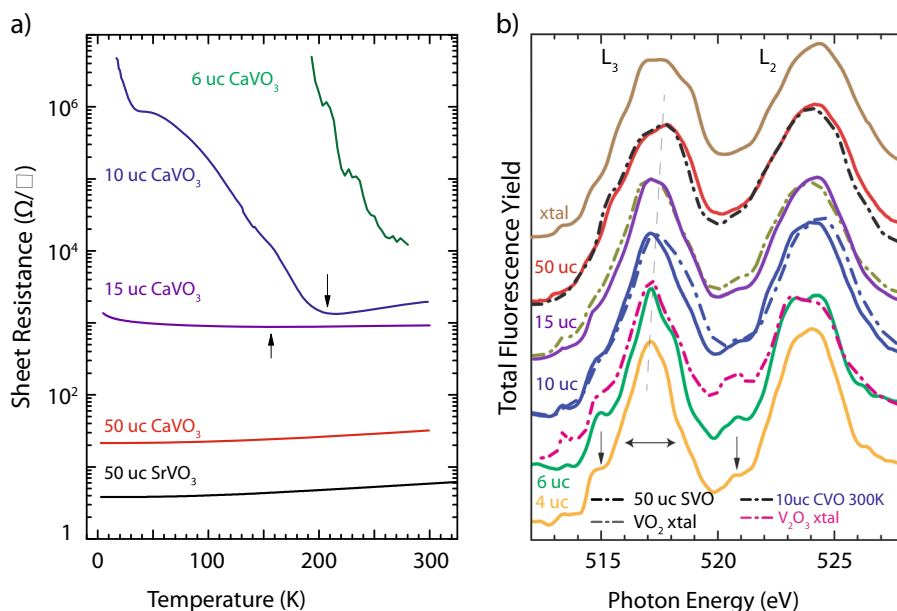
Fig. 2 Reduced electronic bandwidth and increased V^{3+} character across the metal-insulator transition in thin film $CaVO_3$. **a** Resistance as a function of temperature for the samples indicated. Arrows indicate where the slope of the resistance curve reverses sign for the 15 u.c. and 10 u.c. films. **b** X-ray absorption (XAS) as total fluorescence yield for a $CaVO_3$ crystal and films with thicknesses as indicated (solid lines) for π-polarised light at a temperature of 20 K. XAS of the 10 u.c. $CaVO_3$ film at room temperature is shown as a dashed blue curve. XAS is also shown for a 50 u.c. $SrVO_3$ film (dashed black) and VO_2 crystal (dashed grey) and V_2O_3 crystal (dashed magenta)

Control of electronic bandwidth in $CaVO_3$

Figure 3 presents RIXS intensity maps of energy transfer versus incident energy at $T = 20$ K across the V L_3 edge. First, we discuss the energy map for the 50 u.c. $SrVO_3$ and $CaVO_3$ films presented in panels 3a and b. Three fluorescence features,[20] where the energy transfer disperses linearly with incident energy, are evident at higher energy transfers (marked as F1, F2 and F3 in Fig. 3c). These spectral signatures have been observed previously for single crystal $CaVO_3$ and were assigned to, for decreasing energy transfer, a hybridized V–O band (F3), an inter-band transition involving the lower Hubbard band (F2), and an intra-band transition involving a quasiparticle-like band (F1).[21] Furthermore, we observe several new Raman-like modes where the energy transfer is independent of incident energy. We assign the intense Raman mode (R1) located at ~0.3 eV (0.5 eV for $SrVO_3$) to electron-hole pair excitations.[22] The Raman-like scattering at higher energy transfers (R2) is assigned to crystal-field excitations. The assignment of fluorescence and Raman peaks is illustrated in a schematic representation of occupied and unoccupied density of states in Fig. 3e.

The RIXS response undergoes a large change as we traverse the thickness-induced MIT in $CaVO_3$. RIXS maps for insulating 10 and 4 u.c. films are presented in Fig. 3c, d. Our first observation is that the spectral weight in the fluorescence features has decreased relative to the spectral weight in the Raman modes as the film thickness is decreased. This transfer of spectral weight from band to localised excitations is expected as we move from metallic to insulating behaviour. We also observe that the measured peaks become sharper and there is a reduction of the bandwidth of these electronic excitations. The reduced bandwidth of electronic excitations measured across the MIT in our RIXS experiment on $CaVO_3$ is similar to the reduced bandwidth measured using angle-resolved photoemission (ARPES) across the thickness-induced MIT in thin films of another vanadate, $SrVO_3$, that was ascribed to a dimensional crossover below 3–4 u.c.[5] In the case of $CaVO_3$ reported here the crossover occurs at a larger thickness of 10 u.c. suggesting that both strain and dimensionality influence the MIT.

Indeed it has been shown that strain can substantially affect the MIT in other systems, such as $NdNiO_3$.[23]

We quantify the reduction in the bandwidth of the electronic excitations by fitting the data and present the corresponding line cuts and fit results in Fig. 4. The thickness-dependence of the low energy Raman-like RIXS peak that we assign to electron-hole pair excitations[20,22,24] is presented in Fig. 4a. The elastic line has been subtracted and the corresponding fits are presented in S.I. We extract from our fits the bandwidth and energy scale of the electron-hole pair excitations and present these results in Fig. 4c (bottom). The bandwidth is gradually reduced from 0.73 eV in the $SrVO_3$ 50 u.c. film to 0.63 eV in the $CaVO_3$ 50 u.c. film down to 0.38 eV in the insulating 6 and 4 u.c. $CaVO_3$ films. The peak energy exhibits a large jump from 0.5 eV to 0.3 eV from $SrVO_3$ 50 u.c. to $CaVO_3$ 50 u.c. and then is gradually reduced to nearly 0.2 eV in the insulating 6 and 4 u.c. films.

In Figs 4b, c (top) we present line cuts and fit results for the fluorescence features F1 and F2 that are band excitations. We illustrate the origin of the F1 and F2 features in Fig. 3 (bottom) and assign F1 to intra-band excitations involving a quasiparticle-like band and F2 to inter-band excitations involving the lower Hubbard band.[21] The separation between these two RIXS peaks is ~1.8 eV, the same energy separation as the low-energy optical conductivity peaks that were also interpreted as originating from intra- and inter-band excitations. Further support for this interpretation is provided by photoemission spectra that reveal a lower Hubbard band at 1.8 eV below the Fermi level.[25] The total bandwidth of our two measured RIXS peaks, determined from the first derivative of the spectra (shown in S.I.), scales with the bandwidth of the V 3d valence band.[19] Fig. 4c (top) presents the results of this analysis. The total bandwidth displays a sharp drop between the metallic 50 u.c. $CaVO_3$ film (=4 eV) and the 15 u.c. $CaVO_3$ film (=3.5 eV) that is on the verge of being insulating (see Fig. 2a). The bandwidth continues to decrease gradually to 3.2 eV in the most insulating 4 u.c. $CaVO_3$ film. A guide for the eye in Fig. 4b shows the reduction in the separation between intra- and inter-band peaks, consistent with the bandwidth reduction extracted from our derivative analysis. For the 4 u.c. film the relative spectral
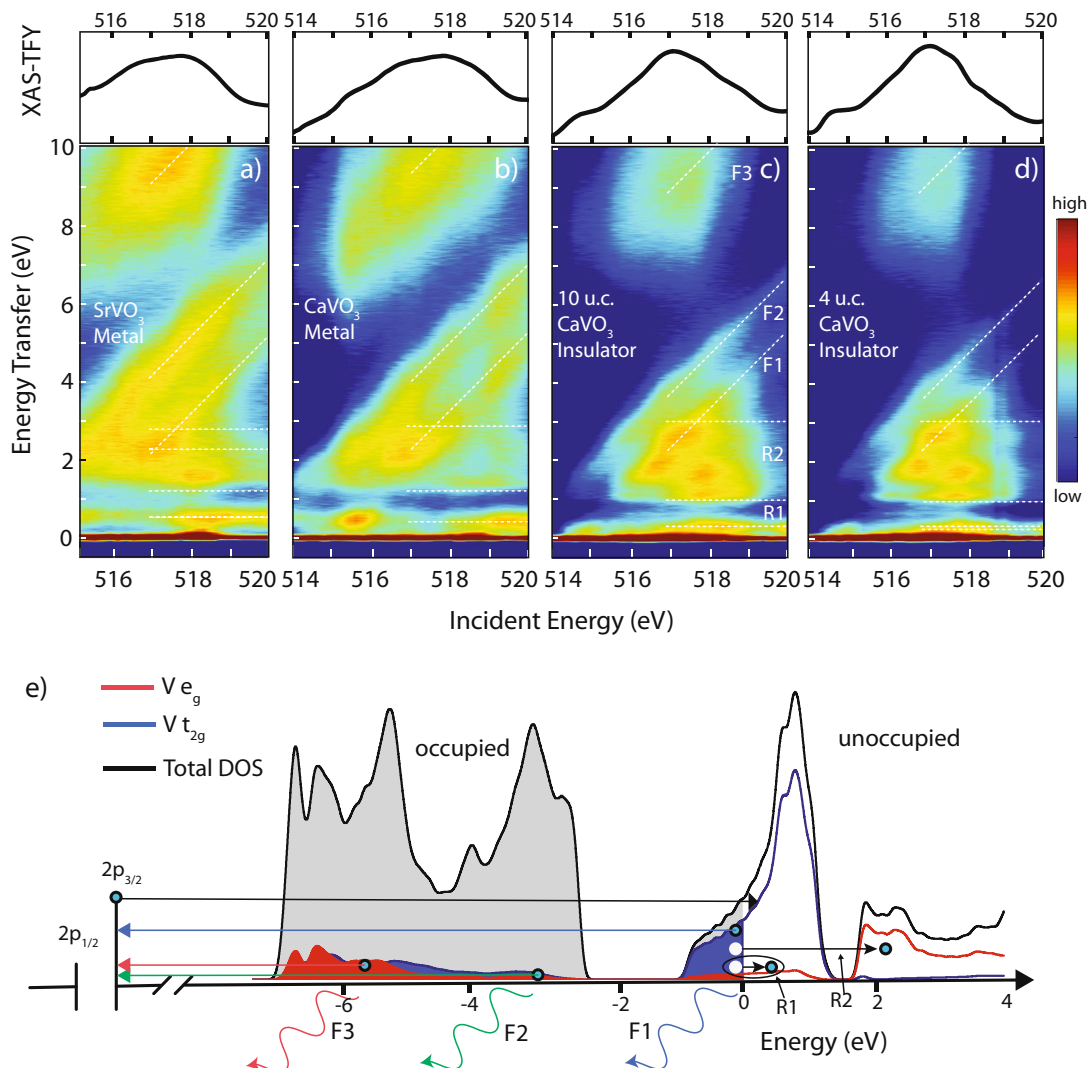
Fig. 3 Overview of resonant inelastic x-ray scattering (RIXS) measurements across a thickness-induced MIT in vanadate thin films. (top) X-ray absorption total fluorescence yield for samples indicated (**a**–**d**). RIXS intensity maps of energy transfer versus incident energy for different film thickness across the thickness-induced MIT. $CaVO_3$ and $SrVO_3$ metal films are 50 unit cells thick. **e** Illustrative sketch of the origin of the Raman and fluorescence peaks measured using RIXS. The sketch is drawn on the total density of states (DOS) and partial DOS for V 3d e_g (red) and V 3d t_{2g} (blue) calculated using density functional theory

weight in the intra-band peak substantially decreases with respect to the inter-band peak (compared to the 50 u.c. $CaVO_3$ film) as the spectral weight is transferred away from the valence band maximum. However, there is still weight in the intra-band peak even in the insulating phase indicating metallic puddles are still present even in the insulating phase.[26]

Local moment formation in $CaVO_3$ films
There are several Raman-like peaks marked as R2 in Fig. 3 and we present line cuts through this region for different film thicknesses in Fig. 5 (left). In the thick metallic 50 u.c. $SrVO_3$ film, that is nominally a perfect cubic structure with no octahedral tilting and formal valence band configuration of V $3d^1$, we observe a broad peak centred around 1.9 eV, a similar energy scale to the t_{2g}-e_g excitations found near 1.7 eV in the insulator YVO_3 with a valence electron configuration of V $3d^2$.[27] For the 50 u.c. $CaVO_3$ film, that has a small orthorhombic distortion and octahedral tilting, we find a large broadening and nearly flat distribution of spectral weight. A three peaks structure is measured in the 15 u.c. $CaVO_3$ film and these peaks continue to sharpen in the insulating 10 u.c., 6 u.c. and

4 u.c. $CaVO_3$ films (Fig. 5 (left)). There are two possible explanations for this reconstruction: strain-induced changes in bond lengths or the formation of local magnetic moments.[27] The effect of epitaxial strain is larger in the thinner films but strain effects are expected to lift the degeneracy of the t_{2g} and e_g states by only a small amount (~100 meV)[15] compared to the large effect reported here. The additional peaks are therefore a clear signature of local moment formation from V^{3+} ions allowing spin flips from a t_{2g}^2 high spin $S = 1$ ground state configuration to configurations involving $S = 0$ and the e_g level.[27] We already have evidence that V^{3+} ions are present in thinner $CaVO_3$ films from our XAS as described earlier and thus we can attribute the additional peak near 1 eV to a local spin flipping t_{2g}^2 $S = 0$ transition at twice the Hund's coupling energy $2J_H$ using the notation of ref. [27] The additional peak near 2.6 eV is also captured by several overlapping local excitations on the V^{3+} ion, namely by transitions to t_{2g}^2 with $S = 0$ of higher crystal-field symmetry and to $t_{2g}^1 e_g^1$ with $S = 1$ or $S = 0$.[27] The formation of a local moment in insulating ultra-thin $CaVO_3$ films starting from a bulk-like non-magnetic thin film is a dramatic effect, resulting from a control of electronic bandwidth and charge redistribution.
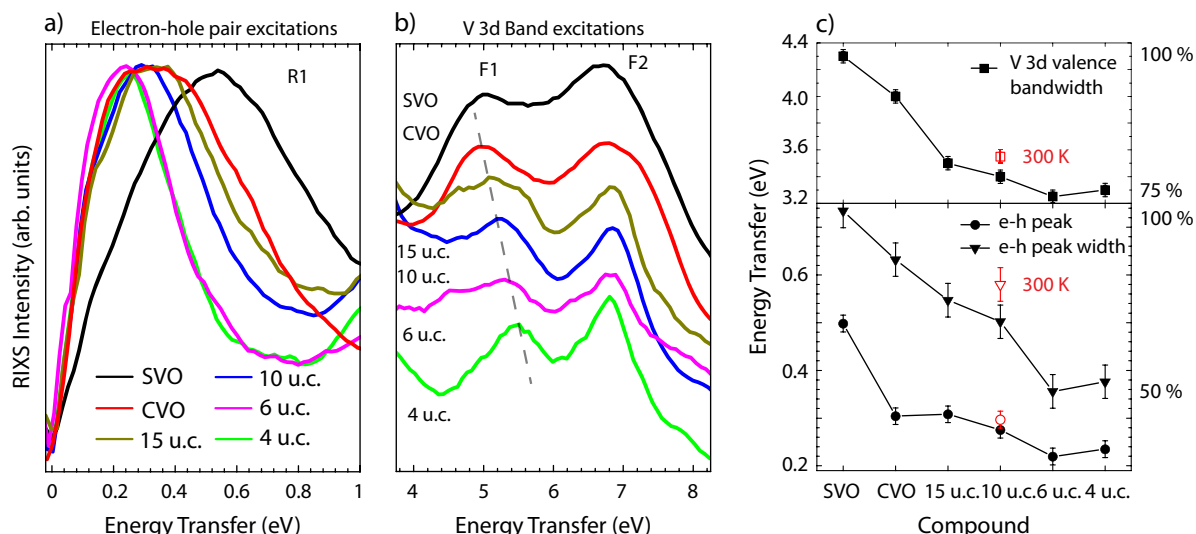
Fig. 4 Forty percent bandwidth reduction across the thickness-induced MIT in $CaVO_3$ thin films. **a**, **b** Resonant inelastic x-ray scattering (RIXS) intensity as a function of energy transfer for the films indicated for an incident energy of 520 eV (in the dip between L_3 and L_2 peaks). $SrVO_3$ and $CaVO_3$ are 50 u.c. films and also shown as 15 u.c., 10 u.c., 6 u.c. and 4 u.c. $CaVO_3$ films. All data were recorded at a temperature of 20 K, and normalized to the total integrated intensity and offset by additive constants for clarity except data in **a** that were multiplied by small factors away from unity for clarity. **c** (top) V 3d bandwidth of the two features F1 and F2 for different films indicated, as extracted from the data presented in **b**; fits for extracting the valence band bandwidth are shown in the supplementary information (S.I.). (bottom) Bandwidth and peak position of the electron-hole pair excitations for different films are indicated, extracted from the fits shown in S.I. Error bars are defined by the standard deviation (SD) of the fits. The empty red square, diamond, and circle represent bandwidth and peak positions extracted from measurements of the 10 u.c. film in the metallic phase at 300 K presented in Fig. 6
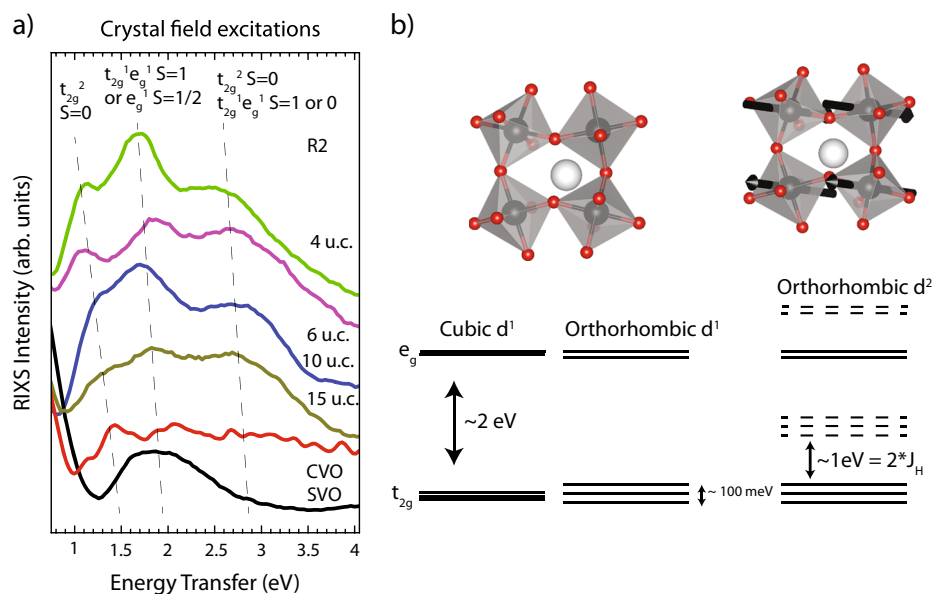

Fig. 5 Reconstruction of crystal field levels across the thickness-induced MIT. **a** Resonant inelastic x-ray scattering (RIXS) intensity as a function of energy transfer for the films indicated for an incident energy of 520 eV (in the dip between L_3 and L_2 peaks). $SrVO_3$ and $CaVO_3$ are 50 u.c. films and also shown are 15 u.c., 10 u.c., 6 u.c. and 4 u.c. $CaVO_3$ films. All data were recorded at a temperature of 20 K, and normalized to the total integrated intensity and offset by additive constants for clarity. Labels indicate the different allowed crystal field excitations for V^{4+} and V^{3+} ions. **b** Schematic of the change in the electronic levels of the V 3d electrons due to reconstruction of the local V site environment and valence occupation

Thermal MIT in 10 u.c. $CaVO_3$ film and the role of V–O hybridization

Now we draw the attention to the MIT which occurs below 220 K in the 10 u.c. $CaVO_3$ film (see Fig. 2a). We present in Fig. 6 the RIXS intensity as a function of energy transfer for the 10 u.c. film in the room temperature metallic phase (at 300 K) and at 20 K, deep in the insulating phase. The change in the RIXS response across the thermal MIT is qualitatively similar to the change for the thickness-induced MIT (see also Fig. 4c): the bandwidth of the electron-hole pair excitation decreases by ca. 15% along with a small softening of the peak position (Fig. 6a), the crystal field levels sharpen (Fig. 6b), and the total bandwidth near the valence band maximum decreases by about 5% (Fig. 6c). In addition, we can quantitatively comment on the relative strength of the high-energy V 3d–O 2p hybridization band shown in Fig. 6d: the intensity of this peak is reduced by 10% in the insulating phase. The reduced V–O
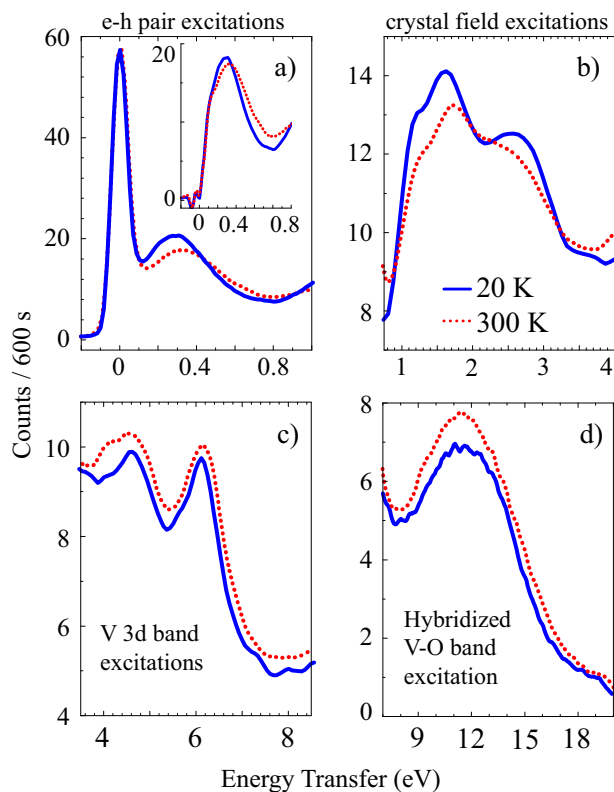
Fig. 6 Resonant inelastic x-ray scattering across the thermal metal-insulator transition in a 10 u.c. CaVO$_3$ film. **a**–**d** Resonant inelastic X-ray scattering (RIXS) intensity as a function of energy transfer at incident photon energy of 520 eV for a 10 u.c. CaVO$_3$ at 20 K and 300 K. (inset of **a**) Same with elastic line subtracted

hybridization across the thermal MIT is comparable to the relative suppression of weight in this hybridized band upon entering the thickness-induced insulating state as shown in Fig. 3 (also see line cuts in S.I. Fig. 7). Thus, the same trend of reduced electronic bandwidth and reduced V–O hybridization is measured in both thermal and thickness-induced MIT, with the effects on the thickness-induced MIT being a factor 2–3 larger.

DISCUSSION

The large reduction of bandwidth in our CaVO$_3$ films is comparable to that realized in the 3d^1 perovskite series SrVO$_3$-CaVO$_3$-LaTiO$_3$-YTiO$_3$ as shown in Fig. 1. The MIT in the latter case is attributed to an increased orthorhombic distortion, and local moment formation, as the cation size is changed.[16] Obviously control of this MIT is chemically complex as it involves substituting two elements, illustrating the usefulness of the additional parameter space enabled by thin film synthesis methods.

We can understand our results by comparing the experimental spectra for the thermal- and thickness-induced MIT. In the thermal MIT case at constant film thickness we still need to consider the epitaxial strain. Strain will induce changes in the V–O bond lengths and V–O overlap/hybridization as experimentally observed in other 3d^1 perovskites.[28] We thus propose that a structural and/or magnetic transition is driving the thermal MIT in our 10 u.c. CaVO$_3$ film as observed in e.g. nickelate films such as NdNiO$_3$.[23] This proposal is supported by the data presented in Fig. 6b that shows a sharpening of crystal field excitations across the thermal MIT. For the thinner CaVO$_3$ films, the electron-hole bandwidth (see Figs. 1 and 4c, d) is sharply reduced moving from 10 u.c. to 6 u.c. and 4 u. c. films. Additionally XAS reveals increasing V 3d^2 contributions

(Fig. 2b) and the crystal field excitations become much shaper for the thickness-induced MIT (Fig. 5).

The increased contribution from V^{3+} ions in the thinner films stems from charge redistribution and is connected to a reduced V–O covalence across the MIT. The reduction of the V 3d bandwidth is driven by a structural reconstruction accompanied by octahedral rotation, that is thereby also changing the V–O hybridization, manifested in an abrupt change of the RHEED patterns of the ultra-thin capped films. In this sense the "electronic localization and bandwidth reduction" as well as the "increase of V^{3+} contributions" are a consequence of the thickness confinement. Oxygen vacancies generated during the growth of CVO films might partially contribute to V^{3+} states, but their amount, in principle, should scale with the film thickness. However, 50 u.c. CVO film does not show more V^{3+} signature in the spectra than thinner CVO films suggesting no significant influence of oxygen vacancies on the properties of the studied CVO films.

The combined effects of charge redistribution, confinement, as well as strain are important in the ultrathin CaVO$_3$ films.[29] Based on the results presented here it is difficult to distinguish which of these effects is the main player driving the thickness-induced MIT. However, we note that the MIT appears to be significantly more complex than the dimensional crossover-driven MIT reported in ultrathin SrVO$_3$ films using ARPES spectroscopy.[5]

Our experiments reveal a bandwidth-driven MIT in CaVO$_3$ films as a function of both thickness and temperature where strain, dimensionality and charge redistribution contribute. A reduced V–O hybridization in the insulating state reveals that the MIT is of Mott-Hubbard type where a d–d gap is opened by a strong Coulomb interaction U between electrons.[30] The sharp thermal MIT observed in our 10 u.c. CaVO$_3$ film should stimulate future work on this model system. Our results are promising for the future of the field of correlated electronics showing that while increased disorder can be present in ultra-thin films, it does not inhibit the Mott physics and related spin or charge ordering. However, we want to emphasise the radical changes in electronic structure that can occur in films of reduced dimensionality, and the importance of including these effects in the rational design of new quantum materials.

METHODS

Experimental details

XAS and RIXS experiments were carried out at the ADRESS beamline of the Swiss Light Source at the Paul Scherrer Institut.[31] All measurements were performed at grazing incidence with the X-rays incident at 15° with respect to the sample surface and with σ or π polarisation. The scattering angle was fixed at 130°. We set the spectrometer[32] in the high throughput configuration using the 1500 lines per mm variable line spacing spherical grating[33] as well as the newly installed CCD camera that provides sub-pixel spatial resolution.[34] The beamline exit slit was 20 μm. The setup yielded a total energy resolution (full width at half maximum) of around 60 meV.

Thin films of CaVO$_3$ and SrVO$_3$ were prepared on SrTiO$_3$ (100) and NdGaO$_3$ (110) substrates respectively by PLD. More information can be found in the supplementary information.

DATA AVAILABILITY

The datasets generated during and/or analysed during the current study are available from the corresponding authors on reasonable request.

AUTHOR CONTRIBUTIONS

M.R. and T.S. conceived the project. D.M.N., M.N., T.S., M.M., C.W.S., E.V.P. and M.R. grew and characterised the thin film samples. D.M.N., X.L., J.P., M.D., V.N.S., M.R. and T. S. carried out the XAS and RIXS experiments. D.M.N., M.R., and T.S. analysed the data. S.B. and C.E. carried out the DFT calculation. D.M.N., M.R., and T.S. wrote the paper with contributions from all authors.

ADDITIONAL INFORMATION

REFERENCES

1. Scherwitzl, R. et al. Metal-insulator transition in ultrathin $LaNiO_3$ films. *Phys. Rev. Lett.* **106**, 246403 (2011).
2. King, P. D. C. et al. Atomic-scale control of competing electronic phases in ultrathin $LaNiO_3$. *Nat. Nano* **9**, 443–447 (2014).
3. Feng, Y. et al. Insulating phase at low temperature in ultrathin $La_{0.8}Sr_{0.2}MnO_3$ films. *Sci. Rep.* **6**, 22382 (2016).
4. Biswas, A., Kim, K.-S. & Yeong, Y. H. Metal-insulator transitions and non-Fermi liquid behaviours in 5d perovskite iridates. Preprint at arXiv:1508.04929v2 (2016).
5. Yoshimatsu, K. et al. Dimensional-crossover-driven metal-insulator transition in $SrVO_3$ ultrathin films. *Phys. Rev. Lett.* **104**, 147601 (2010).
6. Gu, M. et al. Metal-insulator transition induced in $CaVO_3$ thin films. *J. Appl. Phys.* **113**, 133704 (2013).
7. Gu, M., Wolf, S. A. & Lu, J. Two-dimensional Mott insulators in $SrVO_3$ ultrathin films. *Adv. Mater. Interfaces* **1**, 1300126 (2014).
8. Park, S. Y., Kumar, A. & Rabe, K. M. Charge-order-induced ferroelectricity in $LaVO_3$/$SrVO_3$ superlattices. *Phys. Rev. Lett.* **118**, 087602 (2017).
9. Chakalian, J., Freeland, J. W., Millis, A. J., Panagopoulous, C. & Rondinelli, J. M. Colloquium: emergent properties in plane view: strong correlations at oxide interfaces. *Rev. Mod. Phys.* **86**, 1189–1202 (2014).
10. Inoue, I. H., Goto, O., Makino, H., Hussey, N. E. & Ishikawa, M. Bandwidth control in a perovskite-type $3d^1$ correlated metal $Ca_{1-x}Sr_xVO_3$. I. Evolution of the electronic properties and effective mass. *Phys. Rev. B* **58**, 4372–4383 (1998).
11. Maiti, K., Vasanthacharya, N. Y. & Sarma, D. D. Doping dependence of transport and magnetic properties in $La_{1-x}Ca_xVO_3$. *J. Phys. Cond. Mat.* **9**, 7507–7514 (1997).
12. Zhou, J.-S. & Goodenough, J. B. Heterogeneous electronic structure in $CaVO_3$. *Phys. Rev. B* **54**, 13393–13397 (1996).
13. Zhang, L. et al. Correlated metals at transparent conductors. *Nat. Mat.* **15**, 204–210 (2016).
14. Nakano, M. et al. Collective bulk carrier delocalization driven by electrostatic surface charge accumulation. *Nature* **487**, 459–462 (2012).
15. Zhong, Z. et al. Electronics with correlated oxides: $SrVO_3$/$SrTiO_3$ as a Mott transistor. *Phys. Rev. Lett.* **114**, 246401 (2015).
16. Pavarini, E. et al. Mott transition and suppression of orbital fluctuations in orthorhombic $3d^1$ perovskites. *Phys. Rev. Lett.* **92**, 176403 (2004).
17. Nguyen, H. C. & Goodenough, J. B. Localized-itinerant electronic transition in the perovskite system $La_{1-x}Ca_xVO_3$. *Phys. Rev. B* **52**, 8776–8787 (1995).
18. Pen, H. F. et al. Electronic structure of $Y_{1-x}Ca_xVO3$ studied by high-energy spectroscopies. *Phys. Rev. B* **59**, 7422–7432 (1999).
19. Schmitt, T. et al. Resonant soft x-ray emission spectroscopy of V_2O_3, VO_2 and NaV_2O_5. *Surf. Rev. Lett.* **9**, 1369–1374 (2002).
20. Bisogni, V. et al. Ground-state oxygen holes and the metal-insulator transition in the negative charge-transfer rare-earth nickelates. *Nat. Comm.* **7**, 13017 (2016).
21. Laverock, J. et al. Resonant soft x-ray emission as a bulk probe of correlated electron behaviour in metallic $Sr_xCa_{1-x}VO_3$. *Phys. Rev. Lett.* **111**, 047402 (2013).
22. Monney, C. et al. Mapping of electron-hole excitations in the charge-density-wave system $1T$-$TiSe_2$ using resonant inelastic x-ray scattering. *Phys. Rev. Lett.* **109**, 047401 (2012).
23. Dhaka, R. S. et al. Tuning the metal-insulator transition in $NdNiO_3$ heterostructures via Fermi surface instability and spin fluctuations. *Phys. Rev. B* **92**, 035127 (2015).
24. Hancock, J. N. et al. Evidence for core-hole-mediated inelastic x-ray scattering from correlated $Fe_{1.087}Te$. *Phys. Rev. B* **82**, 020513(R) (2010).
25. Inoue, I. H. et al. Systematic development of the spectral function in the $3d^1$ Mott-Hubbard system $Ca_{1-x}Sr_xVO_3$. *Phys. Rev. Lett.* **74**, 2539–2542 (1995).
26. McLeod, A. S. et al. Nanotextured phase coexistence in the correlated insulator V_2O_3. *Nat. Phys.* **13**, 80–86 (2017).
27. Benckiser, E. et al. Orbital superexchange and crystal field simultaneously at play in YVO_3: Resonant inelastic x-ray scattering at the V L edge and the O K edge. *Phys. Rev. B* **88**, 205115 (2013).
28. He, C. et al. Metal-insulator transitions in epitaxial $LaVO_3$ and $LaTiO_3$ films. *Phys. Rev. B* **86**, 081401(R) (2012).
29. Beck, S., Sclauzero, G., Chopra, U. & Ederer, C. Metal-insulator transition in $CaVO_3$ thin films: Interplay between epitaxial strain, dimensional confinement, and surface effects. *Phys. Rev. B* **97**, 075107 (2018).
30. Zaanen, J., Sawatzky, G. A. & Allen, J. W. Band gaps and electronic structure of transition-metal compounds. *Phys. Rev. Lett.* **55**, 418–421 (1985).
31. Strocov, V. N. et al. High-resolution soft X-ray beamline ADRESS at the Swiss Light Source for resonant inelastic X-ray scattering and angle-resolved photoelectron spectroscopies. *J. Synchrotron Rad.* **17**, 631–643 (2010).
32. Ghiringhelli, G. et al. SAXES, a high resolution spectrometer for resonant x-ray emission in the 400–1600 eV energy range. *Rev. Sci. Instr.* **77**, 113108 (2006).
33. Schmitt, T. et al. High-resolution inelastic X-ray scattering with soft X-rays at the ADRESS beamline of the Swiss Light Source: instrumental developments and scientific highlights. *J. Elec. Spec. Rel. Phen.* **188**, 38–46 (2013).
34. Soman, M. R. et al. Developing a CCD camera with high spatial resolution for RIXS in the soft X-ray range. *Nucl. Instrum. Methods Phys. Res. A* **731**, 47–52 (2013).